Spreading and Imbibition of Liquid Droplets on Porous Surfaces

A. Clarke,* T. D. Blake, K. Carruthers, and A. Woodward

Research and Development, Kodak Limited, Headstone Drive, Harrow, Middlesex HA1 4TY, U.K.

Received December 10, 2001. In Final Form: February 11, 2002

By combining a previously developed model of droplet spreading with simple equations to describe liquid penetration, we develop a versatile new model that successfully describes the spreading and imbibition of liquid droplets on porous surfaces. The model is experimentally verified for a range of porous membranes and should be of particular relevance to the interaction of inkjet droplets with porous receivers such as paper.

1. Introduction

The impact and spreading of liquid drops on impermeable solid surfaces is an everyday experience, e.g., raindrops on a windowpane. The topic has been the subject of many experimental and theoretical studies, and much progress has been made recently in explaining the underlying phenomena.[1−4] By contrast, the spreading of liquid drops on porous substrates has received rather less attention,[5,6,7] yet it is, if anything, even more commonplace and important, e.g., raindrops on textiles, spray paint on wood, and inkjet droplets on receivers such as paper. The ink-jet system is especially challenging experimentally, as the drops are very small, typically in the volume range 4−18 pL, and the receivers vary widely in their properties.

In inkjet printing, drops of ink are projected toward the receiver surface at velocities in the range 1−5 m/s. On reaching the surface, the drops start to spread, driven initially by both inertia and capillary forces (Figure 1). The Weber number, *We*, describes the ratio of these forces, and it has been shown[8] that for $We > 50$, splashing will occur. For the inkjet process, *We* is given by

$$We = \rho r v^2/\gamma \qquad (1)$$

with ρ the density, r the radius, v the impingement velocity, and γ the surface tension of the drop. Taking typical values of $\rho = 1000$ kg/m^3, $r = 12$ μm, $v = 2$ m/s, and $\gamma = 30$ mN m^{-1}, *We* is of order 1. Hence, in the initial spreading phase, although inertia is important and waves will be seen on the surface of the drop, no splashing will occur. Furthermore, the momentum will be dissipated very rapidly and capillary forces will dominate thereafter. During this later phase, the drop will exhibit a dynamic advancing contact angle, which will relax toward its static value θ_A as the wetting line slows and eventually stops. As the ink is absorbed, the contact angle will continue to decrease with the wetting line now stationary. When the contact angle falls below its minimum static receding value θ_R, the radius of the remaining drop will begin to decrease and the drop will eventually disappear. Note that we have assumed that the liquid exhibits some degree of contact angle hysteresis, such that $\theta_A > \theta_R$. Such behavior is likely, as receiver surfaces will usually be both rough and heterogeneous.

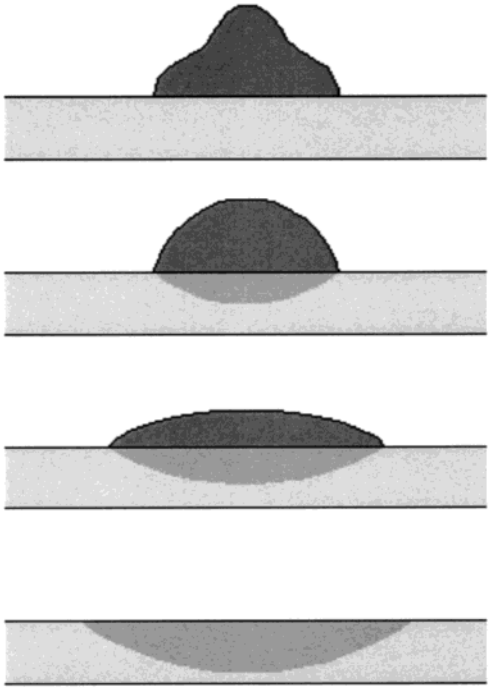

Figure 1. Schematic sequence of behavior for a drop arriving at a solid surface and relaxing to its static advancing contact angle while absorbing into the surface.

A full hydrodynamic analysis of the above sequence of events presents a formidable task. However, recent work on the mechanism of dynamic wetting has led to a very effective model of the relaxation of a sessile drop on an impermeable solid surface.[9] Here, we combine this model with simple equations to describe the imbibition process. This results in a tractable set of equations which suc-

* To whom correspondence should be addressed: Tel: +44 (0)20 8424 5681. Fax: +44 (0)20 8424 3750. E-mail: andrewclarke@kodak.com.

(1) de Ruijter, M. J.; De Coninck, J.; Oshanin, G. *Langmuir* **1999**, *15*, 2209.
(2) de Ruijter, M. J.; Charlot, M.; Voué, M.; De Coninck, J. *Langmuir* **2000**, *13*, 2363.
(3) Rioboo, R.; Tropea, C.; Marengo, M. *Atomization Sprays,* **2001**, *11* (2), 155.
(4) De Coninck, J.; de Ruijter, M. J.; Voué, M. *Curr. Opin. Colloid Interface Sci.* **2001**, *6*, 49.
(5) Kissa, E. *J. Colloid Interface Sci.* **1981** *83*, 265.
(6) Marmur, A. *J. Colloid Interface Sci.* **1988** *124*, 301.
(7) Davis, S. H.; Hocking, L. M. *Phys. Fluids* **1999** *11*, 48.
(8) Range, K.; Feuillebois, F. *J. Colloid Interface Sci.* **1998** *203*, 16.
(9) Blake, T. D.; Clarke, A.; De Coninck, J.; de Ruijter, M. J. *Langmuir* **1997**, *13*, 2164.

10.1021/la0117810 CCC: $22.00
Published on Web 03/12/2002

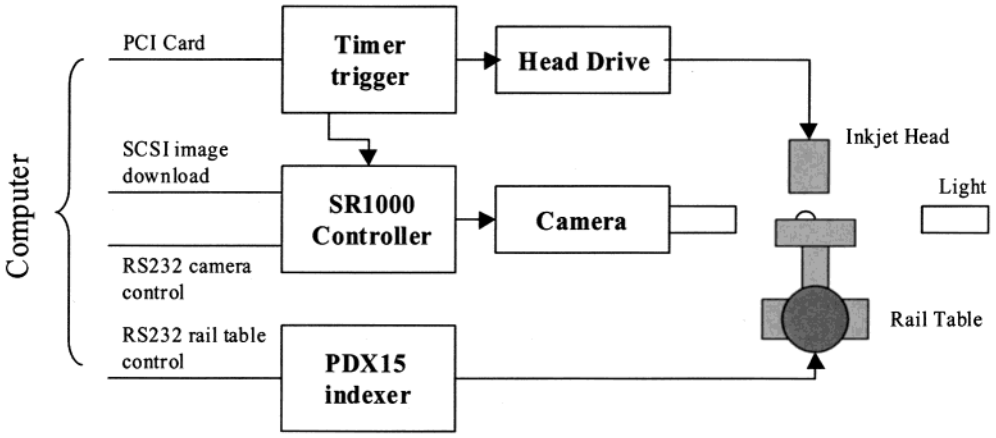

Figure 2. Schematic diagram of the picoliter spreading and absorption, PISA, apparatus.

cessfully model the overall behavior of an inkjet drop as it spreads and absorbs into a porous surface. Comparison with experiment demonstrates the utility of the model.

2. Experimental Section

Following droplet impact, the rate of absorption per unit area, the time to absorb, and the size of the final ink spot are all critically dependent on the interactions between the liquid and the substrate. To understand these interactions and the processes by which ink spreads and imbibes at the surface, it is necessary to have instruments that measure the behavior of droplets at the appropriate length and time scales associated with the inkjet printing process.

To provide suitably detailed information on the interaction of a spreading drop with a receiver surface, a picoliter spreading and absorption (PISA) instrument was developed. A schematic diagram of the arrangement is shown in Figure 2. For the experiments presented here, droplets of the required liquid are supplied from a Hewlett-Packard Thinkjet printer head. A short rail-table and stepper motor are used to translate the sample in the horizontal (x) direction, to position the sample and permit repeat measurements. A collimated tungsten light source provides illumination to silhouette the drop. A high-speed (1000 frames per second) video camera (Kodak SR1000) and a Navitar zoom microscope with a long working distance 10× objective are used to capture the resultant images. These are downloaded to a PC for analysis. Firing of the drops, sample translation, and image capture and analysis are all done under computer control using LabView software.

The PISA instrument is designed to deposit one or more drops and measure both radius and height as a function of time. It is assumed that the drop is axisymmetric and spherical. The height and radius are therefore obtained by fitting a circular arc to the silhouette image of the drop. From the height and radius, the contact angle and volume of the drop are simply derived.

The liquids used in the experiments were water (Millipore Milli-Q plus, viscosity 1.0 mPa s, surface tension 72.4 mN m^{-1}) and an aqueous solution of glycerol (Fischer SLR) and hexelene glycol (Aldrich) (G/HG solution, viscosity 40 mPa s, surface tension 38 mN m^{-1}). The substrates used were commercially available microporous filter membranes made from mixed cellulose esters, specifically MF-Millipore membrane filters: VCWP 090 25, 0.1 μm; GSWP 047 00, 0.22 μm; HAWP 047 00, 0.45 μm; DAWP 047 00, 0.65 μm; AAWP 047 00, 0.8 μm. The quoted dimensions refer to the size of the smallest particles retained and therefore give a lower estimate of the mean pore diameters. In each case the porosity of the materials was very high (0.74−0.82).

3. Spreading and Absorption Model

It has been shown[9] that the relaxation to equilibrium of a liquid drop placed on a smooth substrate is well modeled by the molecular-kinetic theory.[10] This theory leads to the following equation relating the radial velocity of the wetting line to the dynamic contact angle

$$\frac{\partial r}{\partial t} = \frac{2\kappa_S{}^0 h\lambda}{\mu\nu} \sinh\left(\frac{\gamma(\cos(\theta_0) - \cos(\theta))}{2nk_BT}\right) \qquad (2)$$

where $\kappa_S{}^0$ is a molecular jump frequency at n sites of solid/liquid interaction per unit area of the substrate, h is Planck's constant, ν is the molecular volume, λ ($=1/\sqrt{n}$) is the molecular jump length, r is the base radius of the drop, μ is the viscosity, γ is the liquid surface tension, θ_0 is the equilibrium contact angle, θ is the instantaneous dynamic contact angle, k_B is Boltzmann's constant, and T is the temperature. To describe the relaxation of a drop, a second equation that relates the radius to the contact angle is required; this can be obtained by assuming the drop is of constant volume. Thus

$$r = \left[\frac{3V}{\pi} \frac{\sin^3(\theta)}{2 - 3\cos(\theta) + \cos^3(\theta)}\right]^{1/3} \qquad (3)$$

where V is the volume of the drop. Combining eqs 2 and 3 allows us to write differential equations describing the relaxation of the drop to equilibrium. Numerical solution of these equations follows quite straightforwardly.[9]

To model the corresponding process on a porous surface (Figure 3), we have to relax the condition of constant volume, because as drop relaxation occurs the liquid adsorbs into the substrate. Here we use Darcy's law to describe the absorption

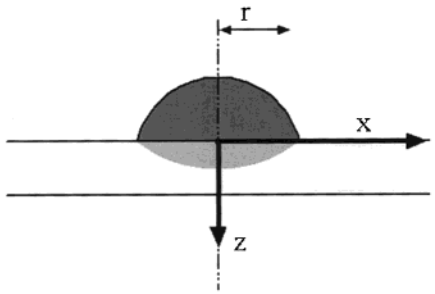

Figure 3. Axes definition for the spread and absorption of a sessile drop at time t. Note that absorption is assumed to be vertical but starts only as the wetting line reaches a given radius, r.

(10) Blake, T. D. In *Wettability*; Berg, J. C., Ed.; Marcel Dekker: New York, 1993.

$$-\nabla p = \frac{\mu}{k} u \tag{4}$$

where ∇p is the pressure gradient, k the permeability, and u the mean liquid velocity in the pore. We assume for simplicity that the porous structure fills vertically, i.e., there is no radial flow within the porous material, and that filling at a particular radius starts when the wetting line reaches that radius. In real systems, radial flow will occur; however its effects will be small for isotropic pore structures, as over the lifetime of the drop, the radius of contact between the drop and the substrate is large compared with the penetration distance. The pressure gradient is therefore the capillary pressure divided by the (vertical) length of filled pore z

$$\nabla p = -\frac{2\gamma \cos(\theta_0)}{az} \tag{5}$$

where a is the effective pore radius. Eliminating ∇p in eqs 4 and 5 leads to a simplified version of the Lucas–Washburn[11,12] equation, which is commonly used to model liquid penetration into porous media. Here, we also assume that the volume of the drop is small compared with the absorptive capacity of the receiver beneath it.

Solving eq 4 in one dimension in combination with (5), the drop volume will behave as

$$\frac{\partial V}{\partial t} = \phi\left(\frac{\gamma k \cos(\theta_0)}{\mu a}\right)^{1/2} \int_0^r 2\pi x \int_{\tau(x)}^t (t - \tau(x))^{-1/2}\, \mathrm{d}t\, \mathrm{d}x \tag{6}$$

where $\tau(x)$ is the time that the pore at radius x started filling and ϕ is the porosity. Unfortunately, at zero time (i.e., $t - \tau = 0$), z goes to zero and so u goes to infinity. We avoid this problem numerically by modifying eq 6 to give a constant meniscus velocity within the pores at short times as follows

$$\frac{\partial V}{\partial t} = \phi\left(\frac{\gamma k \cos(\theta_0)}{\mu a}\right)^{1/2} \times \int_0^r 2\pi x \int_{\tau(x)}^t (t_0 + (t - \tau(x)))^{-1/2}\, \mathrm{d}t\, \mathrm{d}x \tag{7}$$

with t_0 some arbitrarily short offset time. This corresponds to setting a constant initial velocity until enough of the pore has filled and, subsequently, a decreasing pore velocity according to Darcy's law. If we set $t_0 = \rho k/2\mu$, then we recover the universal inertia-driven initial velocity as derived by Bosanquet.[13] Recent molecular dynamics simulations of the early stages of capillary penetration[14] suggest that our approach is physically reasonable.

Eqs 2, 3, and 7 describing droplet spreading with absorption were solved numerically and fitted to data using a code written in Matlab. Note that permeability, pore size, and porosity appear in these equations as a single group, so that they cannot be obtained independently by this analysis.

For diffusive substrates, in which the ink absorbs into, for example, a polymer matrix, Darcy's law can be replaced by the appropriate diffusion equation.

4. Results

Figure 4 shows data for single water drops absorbing into four of the surfaces (nominal pore diameters 0.22–0.8 μm). In each case the drops spread to a radius where the wetting line pinned in less than 5 ms, yielding contact angles between 51° and 83°. Thereafter, absorption proceeded with no further movement of the wetting line.

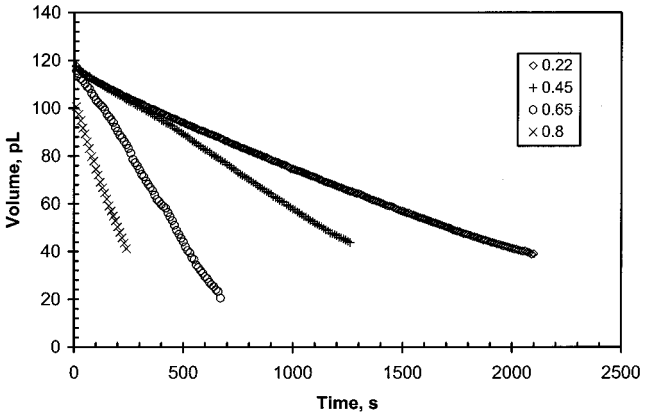

Figure 4. Variation of volume as a function of time for a water droplet on each of four filter membranes having manufacturer's quoted pore sizes of 0.22, 0.45, 0.65, and 0.8 μm. Note the extremely long absorption times.

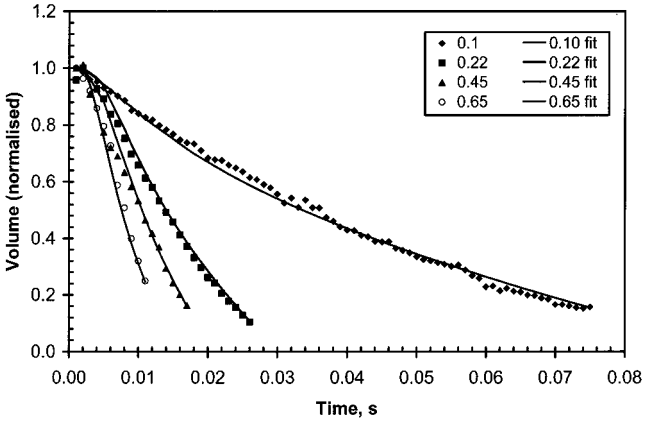

Figure 5. Variation of volume as a function of time for water/glycerol/hexylene glycol droplets on the four smaller filter sizes (0.1, 0.22,, 0.45, and 0.65 μm). The solid lines are the fits to the data. The volumes are normalized to the initial drop volume in each case.

Because of the high rate of spreading, no useful information could be obtained on the dynamic contact angle. In the plot we see that the volume of the drops decrease more-or-less linearly with time. This is surprising since, without spreading, we have only to solve the penetration problem and would therefore expect $\sqrt{t}$ dependence based on the assumption of vertical imbibition. Moreover, the time scale of imbibition is 4 orders of magnitude slower than that observed with lower surface tension liquids (see below). The contact angle data show that these materials are poorly wetted by water. Therefore imbibition may not be the simple uniform process assumed in our model. For example, a poorly wetting liquid will not easily pass from a small to a large pore. Such delays are known to disproportionately influence the overall kinetics of imbibition.[15] Marmur[16] has cited experimental observations in which spontaneous imbibition is arrested for contact angles greater than about 60°.

Figures 5–7 show, respectively, the volume, contact angle and radius for spreading and imbibing drops of G/HG

(11) Lucas, R. *Kolloid Z.* **1918**, *23*, 15.
(12) Washburn, E. W. *Phys. Rev.* **1921** *17*, 273.
(13) Bosanquet, C. H. *Philos. Mag.* **1923** *45*, 525.
(14) Martic, G.; Gentner, F.; Seveno, D.; Coulan, D.; De. Coninck, J.; Blake, T. D. Submitted for publication, 2001.
(15) Ridgway, C. J.; Schoelkopf, J.; Matthews G. P.; Gane, P. A. C.; James, P. W. *J. Colloid Interface Sci.* **2001**, *239*, 417.
(16) Marmur, A. In *Modern Approaches to Wettability*; Schrader, E. M., Loeb, G. I., Eds.; Plenum: New York, 1992.

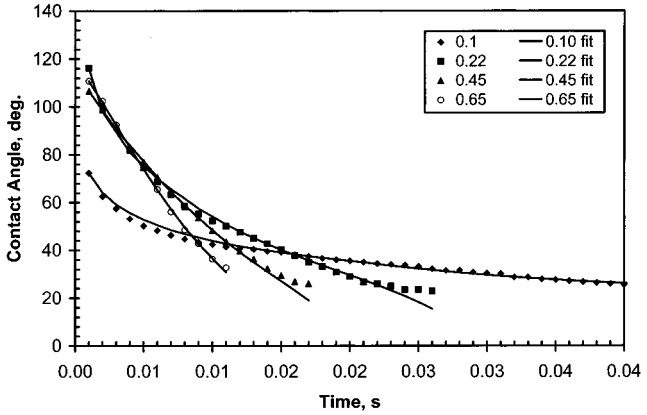

Figure 6. Variation of the contact angle as a function of time for water/glycerol/hexylene glycol droplets on the four smaller filter sizes (0.1, 0.22, 0.45, and 0.65 μm). The solid lines are the fits to the data.

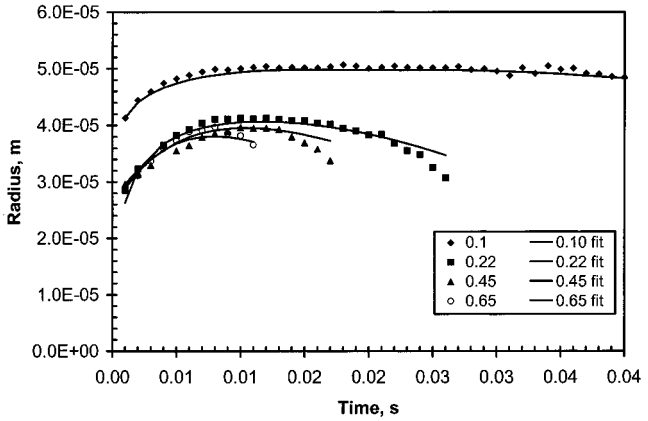

Figure 7. Variation of the radius as a function of time for water/glycerol/hexylene glycol droplets on the four smaller filter sizes (0.1, 0.22, 0.45, and 0.65 μm). The solid lines are the fits to the data.

solution as a function of time on the four substrates with the smaller nominal pore diameters (0.1−0.65 μm). The G/HG solution has a lower surface tension than the water, but a much higher viscosity. Each drop initially spreads to a maximum radius, while the contact angle falls. As imbibition proceeds, the contact angle also falls together with the drop radius. Interestingly, as the radius decreases, the velocity of the wetting line increases. This is reflected in the contact angle, which continues to fall below the fitted static contact angle. Note that this is different behavior to that observed for water drops in Figure 4, where the radius pinned at its maximum extent and contact angle fell as the liquid imbibed.

The data in Figures 5−7 were fitted to our model using a Neder−Mead simplex algorithm provided by Matlab. Since the droplet spreading rate is slow, eq 2 reduces to a linear form with a single "friction" parameter, $\xi = (\mu n k_B T/\kappa_s^0 h\lambda)$. Thus, although the full eq 2 was used in the fitting, there are only three properly independent parameters: a pore scale $\phi^2 k/a$, a friction parameter ξ, and the static advancing contact angle θ_0. Measured values of surface tension and viscosity were used to obtain $\phi^2 k/a$. Note that the permeability $k \propto a^2$,[17] and for the membranes studied $\phi \approx 1$; hence the combined parameter $\phi^2 k/a \propto a$.

Within our model, the same static contact angle is used both externally on the surface of the substrate and within the pores. This may or may not be a good approximation, but any elaboration to allow different angles does not alter the fit numerically, since a change in angle within the pore will simply appear as part of the capillary pressure and be combined within the pore scale $\phi^2 k/a$.

Table 1

	pore size					
parameter	0.10 μm	0.22 μm	0.45 μm	0.65 μm	0.8 μm	units
	Fitted					
ξ	15.9	25.0	23.8	21.5	26.1	Pa s
$\phi^2 k/a$	0.0133	0.0371	0.1133	0.2021	0.2804	μm
θ_0	38.9	48.9	46.7	50.1	51.9	deg
	Calculated from Manufacturer's data					
$\phi^2 k/a$	0.0056	0.0438	0.0752	0.1246	0.1391	μm

The fitted values for all the substrates are listed in Table 1. The friction factor and contact angle are broadly constant, as befits the presumably constant nature of the filter material. The agreement between the fitted value of the pore scale and that calculated from the manufacturer's data is good considering the approximations inherent in modeling complex porous materials, and lends support to the utility of the approach presented here. In addition, there is no reason to expect one-to-one agreement between a pore scale determined from permeability experiments and one that essentially describes filtration efficiency.

In fitting the data, allowance can be made within the model for the effect of contact angle hysteresis. This may be achieved by allowing the static angle to have two values, such that the wetting line advances only when the dynamic contact angle is greater than the static advancing angle θ_A and recedes only when the contact angle falls below the static receding angle θ_R. For the fits presented here, the hysteresis was set to zero except for the 0.1 μm sample, and the contact angle within the pores was taken to be the advancing angle. Close examination of the variation of radius for 0.1 μm sample shows that it initially increases, then for a period remains constant (while the contact angle is still decreasing), before subsequently falling again. For the other samples, the radii increase and then fall, but with no discernible period where the wetting line is stationary.

5. Discussion

In this Letter we have demonstrated that a simple extension to our existing understanding of droplet spreading can be used to model, with good accuracy, the observed behavior of droplets on a porous surface. In particular, the time dependence of the spreading and relaxation process is captured, as well as the time dependence of the volume and the influence of viscosity, though the latter is not shown explicitly here. It is found that the effects of contact angle hysteresis must be included to fit data for some systems.

There is a large difference observed between the low surface tension and high surface tension liquids, with the imbibition process taking more than 2 orders of magnitude longer for the higher surface tension liquid. This can be rationalized as a result of the larger contact angle formed by the higher surface tension liquid. It is well-known that the complex internal geometry of real porous systems inhibits penetration by poorly wetting liquids. With a large contact angle, not all pores are filled, rather a fractal-like wetting front is obtained and the effective porosity and permeability are reduced.[18] Conversely, a liquid with a

(17) Probstein, R. F. *Physicochemical Hydrodynamics*: *an Introduction*; Butterworth: Stonehaven, MA, 1989; pp 98−99.

(18) Cieplak, M.; Robbins, O. M. *Phys. Rev. Lett.* **1988**, *60* (20), 2042.

lower surface tension and contact angle may fill all the pores in the structure completely, yielding a significantly higher permeability.

The model presented above can, of course, be further enhanced by consideration of a full three-dimensional imbibition process or extended by substituting a diffusion model for the Darcy's law pore model.

Acknowledgment. The authors thank Dennis Perchak and Kam Ng for their help with improving the Matlab code used in this work.

LA0117810